Inorganic Chemistry

Article

pubs.acs.org/IC

Ligand Coordination and Spin Crossover in a Nickel Porphyrin Anchored to Mesoporous TiO_2 Thin Films

Darren Achey[†] and Gerald J. Meyer*[,†,‡]

[†]Department of Chemistry and [‡]Department of Materials Science & Engineering, Johns Hopkins University, 3400 North Charles Street, Baltimore, Maryland 21218, United States

S Supporting Information

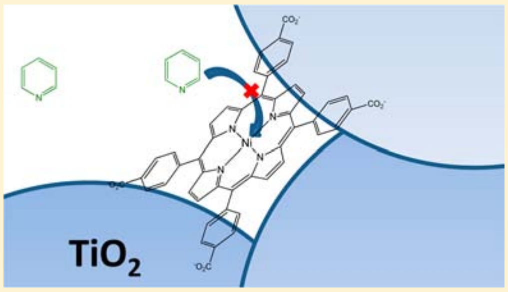

ABSTRACT: The coordination and spin equilibrium of a Ni^{II} *meso*-tetra(4-carboxyphenyl)porphyrin compound, NiP, was quantified both in fluid solution and when anchored to mesoporous, nanocrystalline TiO_2 thin films. This comparison provides insights into the relative rate constants for excited-state injection and ligand field population. In the presence of pyridine, the spectroscopic data were consistent with the presence of equilibrium concentrations of a 4-coordinate low-spin $S = 0$ ($^1A_{1g}$) Ni^{II} compound and a high-spin $S = 1$ ($^3B_{1g}$) 6-coordinate compound. Temperature-dependent equilibrium constants were consistently smaller for the surface-anchored NiP/TiO_2, as were the absolute values of ΔH and ΔS. In the presence of diethylamine (DEA), the ground-state 6-coordinate compound was absent, but evidence for it was present after pulsed light excitation of NiP. Arrhenius analysis of data, measured from −40 to −10 °C, revealed activation energies for ligand dissociation that were the same for the compound in fluid solution and anchored to TiO_2, $E_a = 6.6$ kcal/mol, within experimental error. At higher temperatures, a significantly smaller activation energy of 3.5 kcal/mol was found for $NiP(DEA)_2/TiO_2$. A model is proposed wherein the TiO_2 surface sterically hinders ligand coordination to NiP. The lack of excited-state electron transfer from $Ni^{II}P^*/TiO_2$ indicates that internal conversion to ligand field states was at least 10 times greater than that of excited-state injection into TiO_2.

■ INTRODUCTION

The coordination of ligands to transition metal compounds is influenced by the external environment. Nature has utilized this fact to fine-tune coordination geometries in proteins to optimize electron transfer and catalysis.[1,2] Relatively little is known about such coordination equilibrium at semiconductor interfaces, particularly the mesoporous, nanocrystalline (anatase) TiO_2 materials that have been widely utilized for solar energy conversion applications. A fundamental understanding of coordination chemistry at these interfaces is practically important for applications in photoelectrosynthetic cells that produce electrical power or chemical fuels when irradiated with sunlight.[3] We report herein ligand coordination and spin-crossover behavior of a Ni^{II} porphyrin compound anchored to the aforementioned TiO_2 thin films.

Nickel porphyrin compounds display distinctive excited-state coordination chemistry.[4] Many metalloporphyrins have dissociative excited states whose population leads to ligand-loss photochemistry.[5,6] A well-known example is the dissociation of CO from heme carbonyl compounds.[7] Soret or Q-band excitation generates $\pi-\pi^*$ excited states that undergo internal conversion to dissociative ligand field states, which release CO with a quantum yield of unity under many experimental conditions.[7] In contrast to hemes, light excitation of nickel porphyrins can lead to both dissociative and associative coordination chemistry. For both hemes and nickel porphyrins, the population of the ligand field excited states that drives this coordination chemistry is known to be rapid and occurs on ultrafast time scales.[4] It was, therefore, of interest to see whether these internal conversion processes compete kinetically with excited-state electron injection into TiO_2 that is also known to occur on femto-to-picosecond time scales with rate constants that appear to be sensitive to the experimental conditions.[8−12] Hence, the appearance of light-driven nickel porphyrin coordination chemistry at a TiO_2 interface reports on the time scale of excited-state injection and serves as an internal clock. In one extreme, excited-state injection is rapid, and hence, coordination chemistry would be absent. In the other extreme, where internal conversion is much more rapid than excited-state injection, ligand coordination chemistry similar to that observed in solution would be expected. At the start of these studies, it was unclear which would occur. Recent studies of an isoelectronic (d^8) Co^I porphyrin demonstrated high excited-state injection yields while free base and Zn^{II} porphyrins are known to rapidly inject electrons into TiO_2 from their singlet excited states,[11] suggesting that the same could be true for Ni porphyrins.[13] On the other hand, hemes and iron polypyridyl compounds generally display very low quantum yields for excited-state injection, if they display any at all.[14,15]

Received: May 22, 2013
Published: August 5, 2013

dx.doi.org/10.1021/ic401286a | *Inorg. Chem.* 2013, 52, 9574−9582

A spin change also accompanies ligand, L, coordination to nickel(II) porphyrins (Scheme 1).[16] At high temperatures, the dominant species is low-spin 4-coordinate NiP, while at lower temperatures, high-spin 6-coordinate NiP with two axial ligands is dominant. Excited-state injection from well-defined singlet or triplet inorganic excited states has very little precedence and is of interest in its own right. Therefore, a comparative study is reported herein with NiP and NiP/TiO_2, where P is *meso*-tetra(4-carboxyphenyl)porphyrin. We note that the molecular control of excited-state injection, spin, and coordination number at semiconductor interfaces is important for application in photoelectrosynthetic cells,[3] such as those that one day might generate methane with light, analogous to the nickel cofactor F430 of methyl-coenzyme M reductase in methanogenic Archaea.[17,18]

Scheme 1. Coordination and Spin Equilibria of a Ni^{II} Porphyrin in the Presence of Axial Ligands L

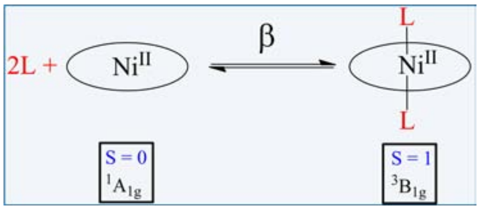

■ EXPERIMENTAL SECTION

Materials. The following reagents were used as received from the indicated commercial suppliers: acetonitrile (Burdick and Jackson, spectrophotometric grade); dimethylsulfoxide (DMSO; Fisher Scientific, 99.9%); pyridine (py; Fisher Scientific, 99.9%); deionized water; acetone (bulk solvent); tetra-*n*-butylammonium hydroxide (TBAOH; Fluka, 1 M aqueous); tetra-*n*-butylammonium perchlorate ($TBAClO_4$; Fluka, >99.9%); lithium perchlorate (Aldrich, 99.99%); argon gas (Airgas, >99.998%); oxygen gas (Airgas, industrial grade); titanium(IV)isopropoxide (Sigma-Aldrich, 97%); fluorine-doped SnO_2-coated glass (FTO; Hartford Glass Co., Inc., 2.3 mm thick, 15 Ω/□); nickel(II) chloride ($NiCl_2$, Sigma-Aldrich, 98%); diethylamine (DEA, Sigma-Aldrich, >99.5%); *N*,*N*-dimethylformamide (DMF, EMD Chemicals, Inc., >99.8%), and *meso*-tetra(4-carboxyphenyl)porphine (P, Frontier Scientific, >97%).

Preparations. *NiP Compound.* A 0.02 g (25 μmol) quantity of *meso*-tetra(4-carboxyphenyl)porphine (P) and 0.035 g (270 μmol) $NiCl_2$ were dissolved in 50 mL of DMSO and heated to ∼170−180 °C for 4 h.[19] Reaction progress was monitored via UV−vis absorption as the four characteristic Q bands of P converted to a single Q band (λ_{max} ∼525 nm) in the nickel *meso*-tetra(4-carboxyphenyl)porphine (NiP) complex.[20] Upon completion of the metal insertion into P, diethyl ether was added to the reaction mixture to precipitate the desired product, NiP. MALDI-MS analysis of NiP measured the expected parent peak of 846 *m*/*z*.

Sensitized Metal Oxide Thin-Film Electrode. Transparent TiO_2 nanocrystallites (anatase, ∼15 nm diameter) were prepared by hydrolysis of Ti(*i*-OPr)$_4$ using a sol−gel technique previously described in the literature.[21] The sols were cast as mesoporous thin films (∼5 μm thick), using Scotch tape as a spacer, by doctor blading onto transparent FTO conductive substrates. Following removal of the tape, the thin films were annealed at 420 °C for 30 min under an atmosphere of O_2 flow.

The films were pretreated with aqueous base (TBAOH, pH ∼11) for 10 min, followed by an acetonitrile wash, and were then immersed in a 50−200 μM NiP/pyridine solution. Within 1 h, the films became brightly colored and were washed thoroughly with pyridine and placed diagonally in a standard 1 cm^2 quartz cuvette containing the experimental solution. The solution was purged with Ar(g) for at least 30 min prior to experimentation. The surface coverage, Γ, in mol/cm^2, was quantified from the measured absorption with the modified Beer−Lambert formula given in eq 1

$$\text{abs} = 1000 * \Gamma * \varepsilon \qquad (1)$$

where ε is the molar decadic extinction (absorption) coefficient, $M^{-1} \cdot cm^{-1}$, that was assumed to be unchanged whether in solution or on the surface. The nickel porphyrins were typically anchored to the films in coverages of $\Gamma = 1{-}4 \times 10^{-9}$ mol/cm^2. The NiP remained anchored to the TiO_2 thin film throughout the experiments.

Spectroscopy. Steady state UV−vis absorption spectra were obtained on either a Varian Cary 50 spectrophotometer or a Hewlett-Packard 8453 photodiode array spectrophotometer. Nanosecond transient absorptions were obtained on an apparatus similar to that which has been previously described.[22] Samples were irradiated with 532 nm light from a frequency doubled, Q-switched, pulsed Nd:YAG laser (Quantel USA (BigSky) Brilliant B; 5−6 ns full width at half-maximum, 1 Hz, ∼10 mm in diameter) directed 45° to the FTO side of a TiO_2 film. The excitation fluence was measured by a thermopile power meter (Molectron) and was typically <2 mJ/cm^2. A 150 W xenon arc lamp served as the probe beam (Applied Photophysics) that was aligned orthogonally to the laser excitation and directed to a monochromator (Spex 1702/04) optically coupled to an R928 photomultiplier tube (Hamamatsu). Transient data were acquired on a computer-interfaced 350 MHz digital oscilloscope (LeCroy 9450). In typical experiments, 30 laser pulses were averaged at each monitoring wavelength, and full spectra were generated by averaging multiple data points.

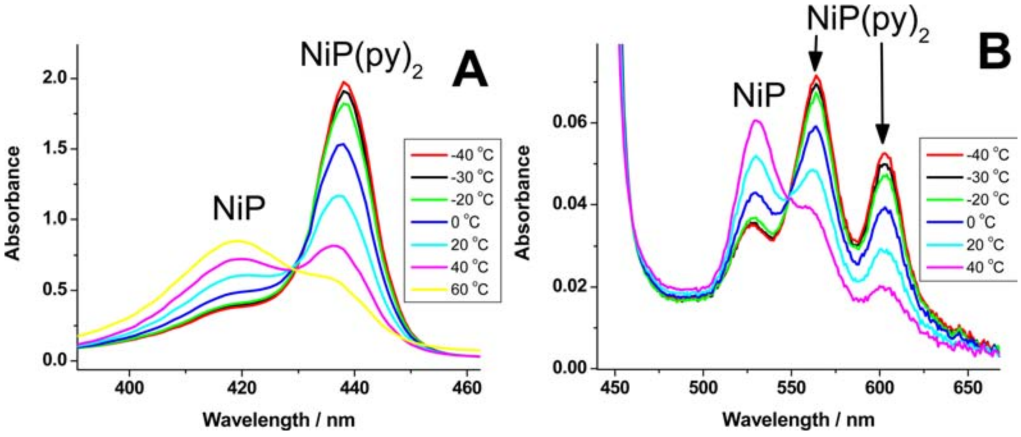

Figure 1. Absorption spectra of NiP in pyridine at the indicated temperatures. (A) Soret band region with λ_{max} = 419 nm assigned to NiP and λ_{max} = 438 nm assigned to NiP$(py)_2$ and (B) Q-band region with λ_{max} = 531 nm for NiP and λ_{max} = 564 and 603 nm for NiP$(py)_2$.

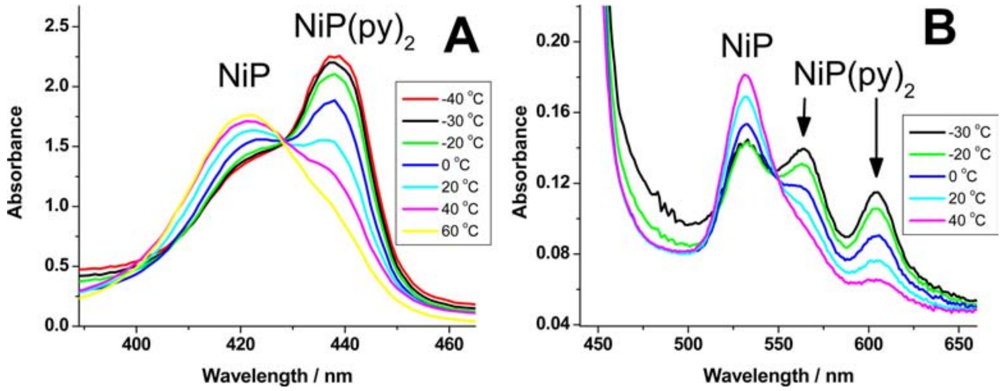

Figure 2. Absorption spectra of NiP/TiO_2 in pyridine at the indicated temperatures. (A) Soret band region with λ_{max} = 421 nm assigned to NiP and λ_{max} = 438 nm assigned to NiP(py)$_2$ and (B) Q-band region with λ_{max} = 531 nm for NiP and λ_{max} = 564 and 603 nm for NiP(py)$_2$.

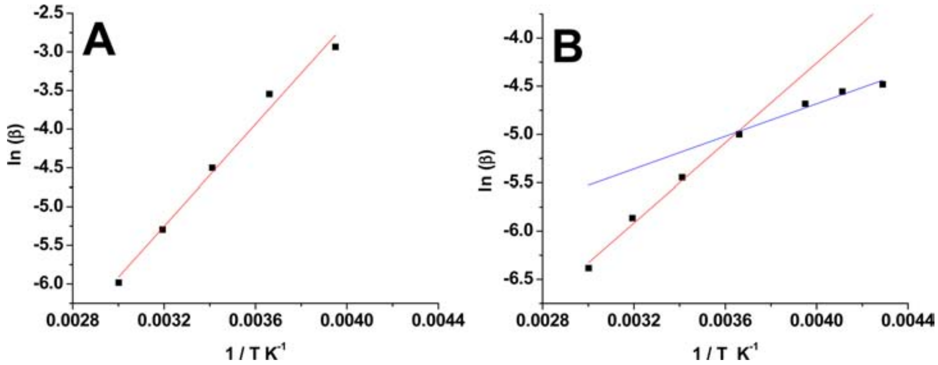

Figure 3. Equilibrium constant data for (A) NiP in pyridine and (B) NiP/TiO_2 in pyridine using the van't Hoff analysis. Overlaid lines are fits to eq 2. In (A), the entire temperature range was fit, while in (B), the data above (red) and below (blue) 0 °C were independently fit.

A liquid nitrogen cryostat (Unisoku CoolSpek USP-203-B) was utilized to achieve control of the temperature. At each temperature, the experimental cuvette was allowed to stabilize for 5 min prior to spectroscopic measurements.

Electrochemistry. Electrochemical measurements utilized a potentiostat (BAS model CV-50W or Epsilon electrochemical analyzer) with a standard three-electrode arrangement with a NiP/TiO_2 thin film deposited on a FTO glass (surface) working electrode, a Pt gauze (Bioanalytical Scientific Instruments, Inc.) counter electrode, and an aqueous Ag/AgCl (KCl saturated) reference electrode. The ferrocenium/ferrocene ($Fe(Cp)_2^{+/0}$) half-wave potential was measured both before and after the experiment in a 100 mM $TBAClO_4$/acetonitrile electrolyte and was used as a standard to calibrate the reference electrode. Conversion to vs NHE was achieved by correcting for the expected ferrocenium/ferrocene $E_{1/2}$ of +310 mV vs the KCl-saturated aqueous calomel electrode (SCE), where SCE is +241 mV vs NHE.[23] All potentials are reported vs NHE unless otherwise noted.

Spectroelectrochemistry was executed through simultaneous application of an applied potential bias while monitoring the UV–vis absorption spectra of TiO_2 thin-film electrodes in the standard electrolytes. At each potential step, a spectrum that was invariant with time was recorded. Single-wavelength absorption features plotted as a function of the applied potential were proportional to the cumulative formation/loss of states; for the $TiO_2(e^-)$ absorption features, this was directly related to the cumulative TiO_2 density of states.[24]

■ RESULTS

Steady-state UV–vis absorption spectra of nickel *meso*-tetra(4-carboxyphenyl)porphyrin (NiP) were measured from −40 °C to +60 °C in neat pyridine solution (~12.4 M), as shown in Figure 1A. Over this temperature range, the Soret band absorption maxima were observed at 419 and 438 nm, the former was predominant at high temperatures and the latter at low temperatures. The Q-band region was also temperature-dependent with one major band at 531 nm at high temperature and two bands that predominated at lower temperatures at 564 and 603 nm (Figure 1B). These spectral changes were reversible upon switching the temperature between the two extremes. The room-temperature absorption spectra of NiP in dimethylformamide (DMF) were in good agreement with that observed at +60 °C in pyridine. Addition of diethylamine to a NiP DMF solution resulted in no significant absorption changes that could be attributed to coordination of diethylamine to NiP.

The Soret and Q-band regions of NiP compounds anchored to mesoporous, nanocrystalline TiO_2 (anatase) thin film, abbreviated as NiP/TiO_2, immersed in neat pyridine, which were recorded over the same temperature range as in solution, are shown in Figure 2. The spectra closely resemble that measured in fluid pyridine solution; however, the absorption bands were broadened (Figure S1), and the sensitivity to temperature was not as great. Absent from the spectroscopic data was any evidence of metal-to-ligand charge-transfer (MLCT) absorption. This was in sharp contrast to what was observed for the isoelectronic Co^IP.[25] Indeed, previous studies of transition metal polypyridyl compounds revealed extinction coefficients for $Ni(bpy)_3^{2+}$ of only 30 $M^{-1}\cdot cm^{-1}$, while that of $Co(bpy)_3^+$ was 5000 $M^{-1}\cdot cm^{-1}$.[26,27]

These two spectra were reasonably assigned to NiP and NiP(py)$_2$ on the basis of comparisons with the literature.[28] The relative concentrations of each compound were abstracted from the absorption data by standard addition of the NiP and

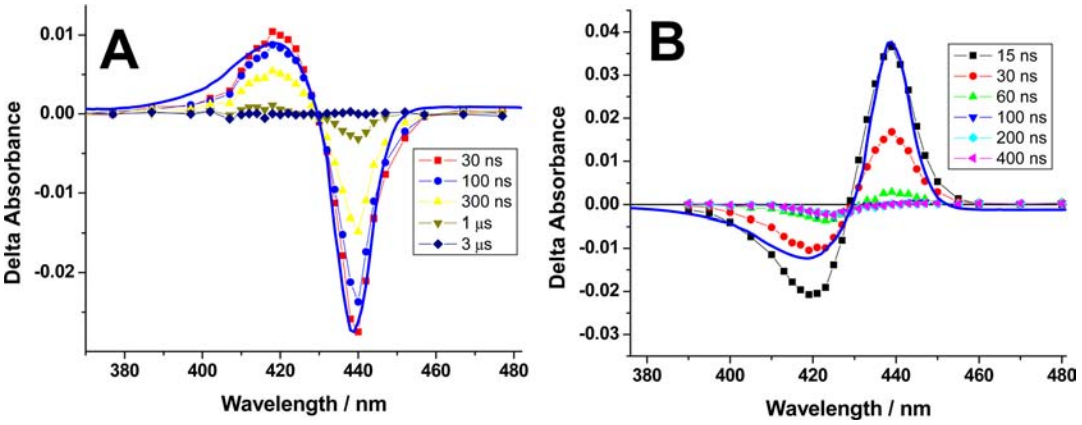

Figure 4. Transient absorption difference spectra measured at the indicated delay times after pulsed 532 nm excitation of NiP in pyridine at −30 °C (A) and +60 °C (B). Overlaid in blue are the expected spectral changes for the (A) dissociation or (B) coordination of pyridine upon light excitation.

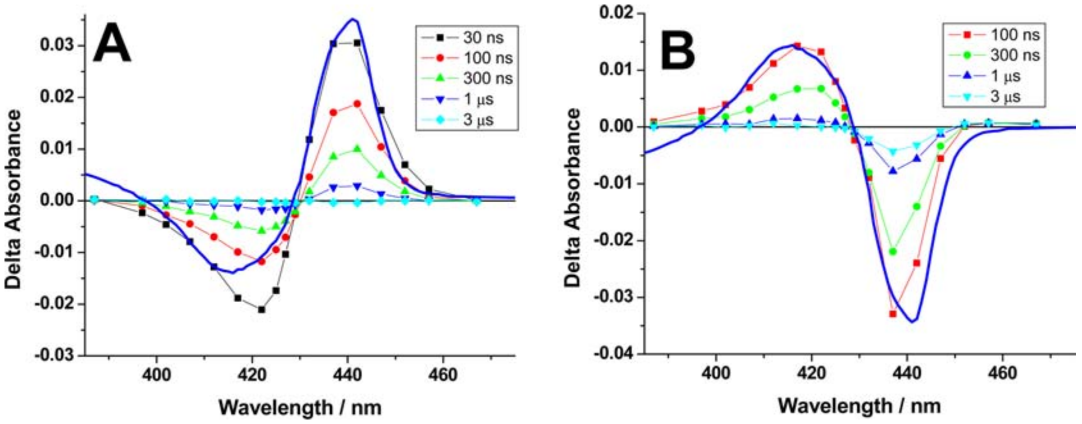

Figure 5. Transient absorption difference spectra measured at the indicated delay times after pulsed light excitation of NiP/TiO_2 in pyridine. The spectra in (A) were measured at −30 °C with 532 nm excitation. The spectra in (B) were measured at −30 °C with 436 nm excitation. Overlaid in blue are the expected spectral changes for the (A) coordination or (B) dissociation of pyridine upon light excitation.

$NiP(py)_2$ spectra. As the experiments were performed in neat pyridine, the $[NiP(py)_2]/[NiP]$ ratio was taken as the equilibrium constant, β. A van't Hoff analysis of the data enabled determination of the enthalpic and entropic parameters, ΔH and ΔS, for the coordination equilibrium, eq 2

$$\ln(\beta) = -\frac{\Delta H}{RT} + \frac{\Delta S}{R} \tag{2}$$

Plots of $\ln(\beta)$ vs $1/T$ were linear for NiP over the temperature range of −20 °C to +60 °C, and values of $\Delta H = -6.5 \pm 0.4$ kcal/mol and $\Delta S = -31.4 \pm 1.4$ cal/mol·K were abstracted from the plots (Figure 3A). However, over the temperature range of −40 °C to +60 °C, the spectroscopic data for NiP/TiO_2 were nonlinear (Figure 3B). The data were satisfactorily modeled when a more limited temperature range was utilized. From −40 to 0 °C, values of $\Delta H = -1.7 \pm 0.2$ kcal/mol and $\Delta S = -16.1 \pm 1.0$ cal/mol·K were abstracted, while $\Delta H = -4.1 \pm 0.3$ kcal/mol and $\Delta S = -24.8 \pm 1.0$ cal/mol·K were obtained for the higher 0 °C to +60 °C temperature range.

Figure 4 shows transient absorption difference spectra measured at the indicated delay times after pulsed laser excitation of NiP in neat pyridine at −30 °C (A) and +60 °C (B). The spectra were the same when they were normalized, indicating that only one species was being generated with light. Simulations based on the steady-state absorption measured as a function of temperature are overlaid. At −30 °C, the overlaid difference spectrum corresponded to the photogeneration of NiP from $NiP(py)_2$, while at +60 °C, spectra were fully consistent with the generation of $NiP(py)_2$ from NiP. The spectra decayed cleanly to the baseline, and steady-state absorption measurements before and after laser photolysis showed no evidence of permanent photochemistry. Pulsed laser excitation of NiP in 1 M diethylamine DMF solutions resulted in transient absorption changes that were reasonably assigned to the coordination of two diethylamines as axial ligands to NiP (Figure S2A). The transient absorption difference spectra were invariant with temperature, but the kinetics were temperature-dependent.

Figure 5 displays transient absorption difference spectra measured at the indicated delay times after pulsed laser excitation of NiP/TiO_2 in neat pyridine at −30 °C with 532 nm excitation (A) and −30 °C with 436 nm excitation (B). Interestingly, with 532 nm excitation, the difference spectra collected were consistent with the photogeneration of $NiP(py)_2$ from NiP at all temperatures, as shown in Figures S3 and 5A. This was in contrast to that measured in fluid solution because the equilibrium concentration of NiP at −30 °C was higher in the mesoporous thin films than it was in fluid solution. However, 436 nm light more selectively excited $NiP(py)_2/TiO_2$ than NiP/TiO_2, and hence, spectral data consistent with net dissociation of the pyridine ligands were observed (Figure 5B). Pulsed laser excitation of NiP/TiO_2 in DMF solutions that

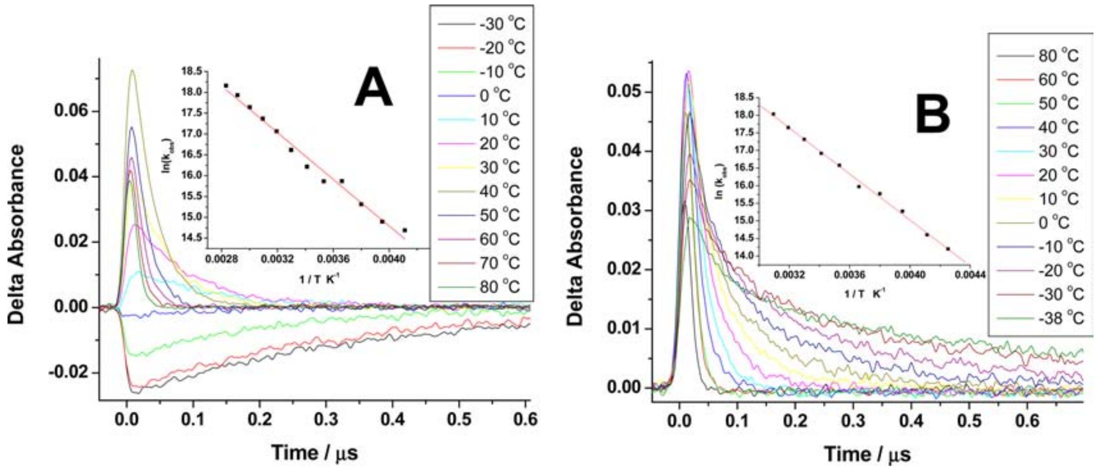

Figure 6. Transient absorption changes measured after pulsed 532 nm excitation of (A) NiP at 440 nm and (B) NiP/TiO_2 at 445 nm in pyridine at the indicated temperatures. The insets show Arrhenius analysis of these same data.

contained diethylamine resulted in absorption changes consistent with those observed in fluid solution (Figure S2B). Under the same laser irradiance conditions, pulsed laser excitation of NiP/TiO_2 in 0.1 M $LiClO_4$ in acetonitrile yielded no observable transient absorption changes.

The transient absorption data measured in fluid solutions were well-described by a first-order kinetic model. The abstracted rate constants were independent of the monitoring wavelength. The temperature-dependent rate constants were fit to a modified Arrhenius expression, eq 3

$$\ln(k_{obs}) = -\frac{E_a}{R^*T} + \ln(A) \tag{3}$$

Kinetic data and an Arrhenius plot for NiP in pyridine are shown in Figure 6A. An activation energy, $E_a = 5.6 \pm 0.2$ kcal/mol, and a pre-exponential factor, $A = 2.0 \pm 0.8 \times 10^{11}$, were abstracted. The kinetic data measured after pulsed laser excitation of NiP/TiO_2 in pyridine also followed a first-order kinetic model when the temperature was greater than +40 °C (Figure 6B).

At cooler temperatures, the data were clearly nonexponential and were well-described by a sum of two first-order rate constants (i.e., a biexponential kinetic model). For data measured at these temperatures, an average lifetime was calculated, eq 4, where α_1 and α_2 represent the relative amplitudes of the first and second lifetimes, τ_1 and τ_2.

$$\frac{1}{k_{obs}} \approx \tau_{avg} = \frac{\alpha_1\tau_1^2 + \alpha_2\tau_2^2}{\alpha_1\tau_1 + \alpha_2\tau_2} \tag{4}$$

The reciprocal of τ_{avg} was taken as an estimate of k_{obs}. The kinetic data and Arrhenius analysis are shown in Figure 6B from which values of $E_a = 6.5 \pm 0.1$ kcal/mol and $A = 1.6 \pm 0.4 \times 10^{12}$ s^{-1} were abstracted. Likewise, the kinetic data measured after light excitation of NiP/TiO_2 in 9.7 M diethylamine solution were exponential at temperatures above −10 °C and nonexponential at lower temperatures. The lower temperature data were again fit to a biexponential kinetic model, and an average rate constant was calculated and utilized as k_{obs} for the Arrhenius analysis.

Arrhenius analysis of the observed rate constants measured after pulsed light excitation of NiP in 1 M diethylamine DMF solutions yielded activation parameters of $E_a = 6.6 \pm 0.1$ kcal/mol and $A = 4.4 \pm 0.9 \times 10^{12}$ (Figure 7). The Arrhenius analysis of NiP/TiO_2 in 9.7 M diethylamine over the two temperature ranges (40 °C to −10 °C and −10 °C to −40 °C) yielded $E_a = 3.5 \pm 0.1$ kcal/mol, $A = 2.5 \pm 0.6 \times 10^{10}$ and $E_a = 6.9 \pm 0.6$ kcal/mol, $A = 2 \pm 3 \times 10^{13}$, respectively. All of the thermodynamic and activational parameters are given in Table 1, as well as selected literature values.

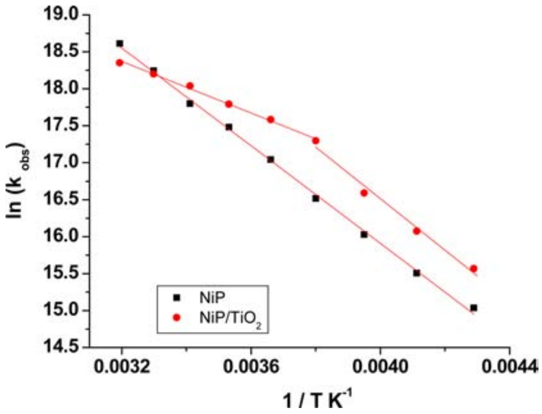

Figure 7. Temperature-dependent Arrhenius analysis of NiP in 1 M diethylamine in DMF (black) and NiP/TiO_2 (red) in 9.7 M diethylamine of the observed rate of transient signal decay at 435 nm.

A NiP/TiO_2 thin film immersed in 0.1 M $TBAClO_4$ in pyridine was used as the working electrode in a standard three-electrode electrochemical cell positioned in a 1 cm cuvette in a UV–vis spectrophotometer. Forward (negative) bias raised the Fermi level of the functionalized film, which prompted the appearance of the absorption features characteristic of reduced TiO_2, abbreviated as $TiO_2(e^-)$, Figure S4.[29] As the Fermi level was further increased, an increase in the $TiO_2(e^-)$ absorption feature was observed. The absorption data were converted to Γ, mol/cm^2, using the modified Beer's Law, eq 1, with an extinction coefficient of 1000 $M^{-1}\cdot cm^{-1}$ at 800 nm. The $TiO_2(e^-)$ concentration increased exponentially with the negative applied bias. The concentrations were multiplied by Faraday's constant to receive units of mC/cm^2, and the data were fit to an exponential function. The derivative of this function, with respect to voltage, resulted in the chemical capacitance (mF/cm^2).[24]

Table 1. Thermodynamic and Activational Parameters for Nickel Porphyrins

	ΔH (kcal/mol)	ΔS (cal mol^{-1}·K^{-1})	E_a (kcal/mol)	A (s^{-1})
NiP/pyridine	-6.5 ± 0.4	-31.4 ± 1.4	5.6 ± 0.2	$2.0 \pm 0.8 \times 10^{11}$
NiP/TiO_2/pyridine			6.5 ± 0.1	$1.6 \pm 0.4 \times 10^{12}$
NiP/TiO_2/pyridine (temp < 0 °C)	-1.7 ± 0.2	-16.1 ± 1.0		
NiP/TiO_2/pyridine (temp > 0 °C)	-4.1 ± 0.3	-24.8 ± 1.0		
NiTPP/pyridine[a]	-5.3 ± 0.4	-31.5 ± 0.3		
NiTPP/piperidine[b]	-5.6 ± 0.5	-21 ± 2		
NiTPP/DEA[c]			4.5	1.5×10^{11}
NiP/DEA			6.6 ± 0.1	$4.4 \pm 0.9 \times 10^{12}$
NiP/TiO_2/DEA (temp > −10 °C)			3.5 ± 0.1	$2.5 \pm 0.6 \times 10^{10}$
NiP/TiO_2/DEA (temp < −10 °C)			6.9 ± 0.6	$2 \pm 3 \times 10^{13}$

[a] Data from ref 43, where TPP is tetraphenylporphyrin. [b] Data from ref 28, where TPP is tetraphenylporphyrin. [c] Data from ref 42, where TPP is tetraphenylporphyrin.

■ DISCUSSION

The overall spin and coordination equilibrium constant β depicted in Scheme 1 has been proposed to represent the product of two stepwise formation constants, $\beta = K_1K_2$, as shown in Scheme 2.[30]

Scheme 2. Two Stepwise Formation Constants for Ligand Coordination to NiP

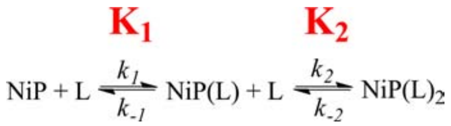

A 5-coordinate intermediate has thus been invoked, even though it was not observed in this study nor has it been clearly identified elsewhere, although a recent publication suggests its presence when a single axial ligand is covalently bonded to the porphyrin ring.[31] Based on related heme chemistry, it seems likely that the second formation constant is much larger than the first, $K_2 \gg K_1$, such that the steady-state concentration of the putative 5-coordinate species is sufficiently low that it could not be detected spectroscopically.[32−34]

Holten and co-workers and others have found that the axial coordination of ligands to nickel porphyrins can be induced with light and have proposed a mechanism for this.[4,35,36] Likewise, dissociation of ligands from nickel porphyrins can be induced with light. Magnetic data have clearly shown that a spin change from $S = 0$ to $S = 1$ accompanies the change in coordination number.[31,37] Chen and co-workers have directly observed the coordination environment of a related nickel porphyrin through novel X-ray transient absorption measurements.[38] Here, we build on this prior literature and examine the influence of a semiconductor surface on this well-characterized spin and coordination equilibrium. The mesoporous, nanocrystalline TiO_2 thin films commonly utilized in dye sensitized solar cells were employed as the semiconducting material as they enable spectroscopic measurements to be made with high signal-to-noise ratios and are good acceptors for excited-state electron transfer.[39] To our knowledge, this is the first study where spin and coordination number of a molecular compound can be controlled simultaneously on a semiconductor surface.[15,40,41] For the purposes of discussion, we assume that the equilibria shown in Scheme 2 are operative for ligand coordination to NiP in fluid solution and within the mesopores of the nanocrystalline TiO_2 thin films. While the spectroscopic data reported herein gives no direct information on the spin change that is known to accompany ligand coordination, the similarity of the spectral data with those reported previously strongly suggest that it is operative.

Kinetics. Laser flash photolysis of Ni porphyrins in the presence of ligands is known to produce nonequilibrium concentrations of the 4- and 6-coordinate species.[4] The observed rate constant, k_{obs}, for return to equilibrium thus reports on the kinetics and mechanism(s) for NiP coordination, behavior that we have exploited here. However, the relationship between k_{obs} and the elementary rate constants given in Scheme 2 is complicated, and without knowledge of the rate limiting step, assumptions must be made. We, therefore, employed the approach of Hoshino and co-workers, who found that secondary amines only coordinate to nickel porphyrins in the excited state, not in the ground state.[42] The insensitivity of the observed rate constants to amine concentration led to the reasonable conclusion that amine dissociation from the 6-coordinate complex was the rate-limiting step, eq 5

$$\mathrm{NiP(DEA)_2} \xrightarrow{k_{-2}} \mathrm{NiP(DEA)} + \mathrm{DEA} \qquad (5)$$

In agreement with this report,[42] there was no evidence of diethylamine coordination to NiP or NiP/TiO_2 in the ground state, but it was generated after pulsed laser excitation. The activation barrier for amine dissociation was measured to be 6.6 ± 0.1 kcal/mol in fluid solution with a frequency factor of $4.4 \pm 0.9 \times 10^{12}$ s^{-1}. When anchored to the mesoporous thin film, the activation energy below −10 °C had increased uncertainty due to the limited number of data points and the appearance of nonexponential kinetics. Nevertheless, the value was within experimental error the same, $E_a = 6.9 \pm 0.6$ kcal/mol, as that measured in fluid solution. A significantly smaller activation energy for ligand dissociation, $E_a = 3.5 \pm 0.6$ kcal/mol, was abstracted from kinetic measurements above −10 °C. The smaller activation energy implies that the ligands were more weakly coordinated to the Ni^{II} center within the mesoporous thin films, as was also inferred by the smaller equilibrium constants discussed below.

Thermodynamics. The thermodynamic parameters for pyridine coordination were abstracted from the spectroscopically measured equilibrium constants through a van't Hoff analysis. The equilibrium from left to right was enthalpically favored as two Ni−N bonds were formed and was entropically disfavored as three molecules reacted to form one. The $\Delta H = -6.5$ kcal/mol and $\Delta S = -31$ cal/(mol K) values abstracted were qualitatively consistent with this model and were similar to those previously reported for a related Ni porphyrin.[42,43]

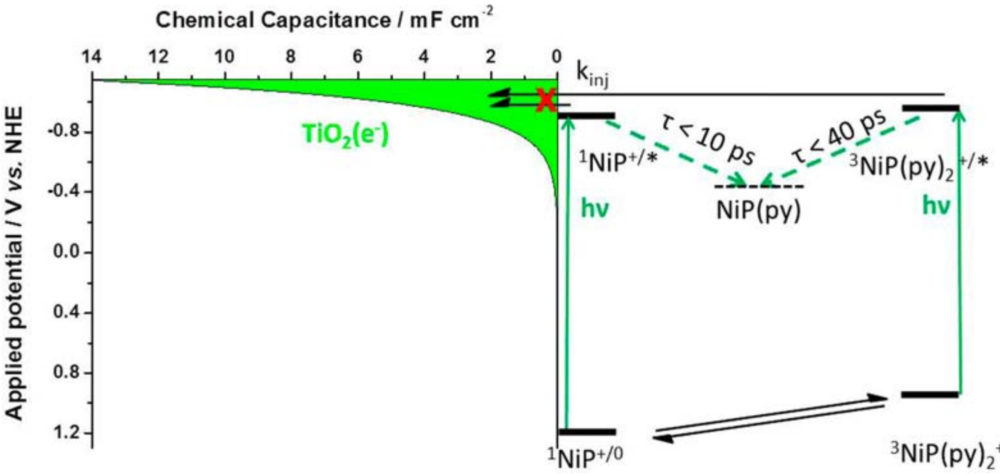

Figure 8. Chemical capacitance of a NiP/TiO_2 thin-film electrode immersed in 0.1 M $TBAClO_4$/pyridine as a function of applied potential. The ground- and excited-state reduction and the lifetimes were taken from the literature, as is described in the text.[20]

The influence of the mesoporous thin film on pyridine coordination equilibrium was significant. At any given temperature from −40 to +60 °C, the overall equilibrium constants were smaller than that measured in fluid pyridine solution. Quantitative comparisons were complicated by the appearance of nonlinear van't Hoff plots. At temperatures above 0 °C, the absolute values of ΔH and ΔS were about 2/3 lower for the surface-anchored porphyrin. Below 0 °C, the equilibrium constants became much less temperature-dependent with significantly smaller absolute values of ΔH and ΔS. Assuming that the Ni-pyridine coordination represents the principle contribution to the enthalpy change, these data suggest that the Ni−N bonds are weaker when the metalloporphyrin was anchored to the TiO_2 nanocrystallites. This suggested that the presence of the TiO_2 surface sterically influences Ni−N bond lengths and angles away from the optimal fluid solution values. These sterics may result in a distribution of equilibrium constants that can be adequately modeled by two discrete values. As the temperature was lowered from +60 °C, those metalloporphyrins that were well-solvated would likely be the first to coordinate pyridine with thermodynamic parameters most similar to that measured in fluid solution. When the temperature was lowered further, pyridine coordination to those metalloporphyrins located within more sterically confined regions of the mesoporous thin film, such as the necking regions between TiO_2 nanocrystallites, occurs. The broadened absorption spectra measured for the surface-anchored NiP suggest a distribution of environments as do the nonexponential kinetics for ligand dissociation observed at low temperatures.

Relevance to Excited-State Injection. As mentioned in the Introduction, the appearance of light-initiated NiP/TiO_2 coordination chemistry reports on the time scale for excited-state injection. Since there was no evidence for excited-state injection, a possible conclusion is that internal conversion was far more rapid than was excited-state injection. The question is why? One possibility is that the NiP excited states simply were not strong enough photoreductants to inject electrons into TiO_2. To test this, the spectroelectrochemical reduction of TiO_2 was measured, and this evidence, along with literature values of NiTPP, where TPP is *meso*-tetra-phenylporphyrin, redox chemistry, and the spectroscopic data reported herein enabled the interfacial scheme shown in Figure 8 to be constructed.

Attempts to oxidize NiP/TiO_2 were unsuccessful. However, Kadish reported the quasi-reversible room-temperature reduction potentials of $NiTPP^{+/0}$ in DMF and $NiTPP(py)_2^{+/0}$ in pyridine to be +0.96 and +0.69 V vs SCE that correspond to +1.20 and +0.93 V vs NHE, respectively.[20] The reducing power of the NiP and $NiP(py)_2$ excited states was then calculated through a thermodynamic cycle with the free energy in the excited state, ΔG_{es}, eq 6

$$E^\circ(NiP^{+/*}) = E^\circ(NiP^{+/0}) - \Delta G_{es} \quad (6)$$

To estimate ΔG_{es}, the long wavelength Q-band absorption onset was utilized. This approach appears to be reasonable as porphyrins generally exhibit small Stokes shifts between the absorption and fluorescence.[44]

With these assumptions, both excited states are potent photoreductants, E° ($NiP^{+/*}$) = −0.94 V and E° ($NiP(py)_2^{+/*}$) = −0.98 V vs NHE. Related ruthenium and organic dyes with similar reduction potentials do indeed quantitatively inject electrons into TiO_2.[45−47] Furthermore, the spectroelectrochemical data reported herein revealed a high density of TiO_2 acceptor states at these potentials. The pyridine electrolyte did, in fact, result in a lower density of states than did the more commonly used LiI/CH_3CN.[25,29] However, light excitation of NiP/TiO_2 in $LiClO_4$/CH_3CN did not result in a significant excited-state injection yield. Therefore, the lack of excited-state injection for $^1NiP^*$ or $^3NiP(py)_2^*$ does not emanate from unfavorable thermodynamics and must be kinetic in origin.

With a 130 fs time resolution, Rodgers and co-workers showed that internal conversion to ligand field states of NiTPP in toluene was complete in less than 1 ps.[48] Likewise, Holten and co-workers found that this occurred in less than 40 ps for $NiTPP(py)_2$.[4] Durrant and co-workers reported that in less than 100 fs over 30% of the ZnP* and H_2P^* excited states had injected electrons into TiO_2.[11] If these internal conversion values measured in fluid solution translated to the TiO_2 interface, an injection yield of at least 30% would be expected, contrary to what was observed. Since an injection yield of 10% could easily be measured under these experimental conditions, the ratio of rate constants for internal conversion to excited-state injection must be greater than 10 (ie., $(k_{ic})/(k_{inj}) > 10$). Assuming Durrant's data are relevant to NiP*/TiO_2, internal conversion to the ligand field states would have to occur on a ~10 fs time scale to be consistent with the data reported herein. Likewise, if internal conversion occurred on a ~1 ps time scale, injection would have to be slower than 10 ps. Since ZnP/TiO_2 seems to be a reasonable model for NiP/TiO_2 and the activation to ligand field states is known to be environmentally sensitive,[41,49−53] we favor a model wherein internal conversion of the NiP and $NiP(py)_2$ excited states occurs on a faster time scale than electron injection at these TiO_2 interfaces.

CONCLUSIONS

Spin and coordination equilibrium of a Ni^{II} porphyrin compound at semiconductor interfaces has been characterized for the first time. The mesoporous, nanocrystalline TiO_2 semiconductor thin films employed enabled the equilibrium and kinetics to be quantified spectroscopically. Relative to fluid solution, the surface-anchored porphyrin displayed smaller equilibrium constants for pyridine coordination that resulted from smaller absolute values of ΔH and ΔS. The activation energy for amine dissociation was also smaller, as revealed by temperature-dependent kinetic measurements. The data were consistent with a model wherein a distribution of NiP environments exists within the TiO_2 thin film, a significant fraction of which presents steric hindrance to amine coordination. The lack of excited-state injection by NiP^*/TiO_2 suggests that internal conversion to ligand field states occurs on a femtosecond time scale.

ASSOCIATED CONTENT

Supporting Information

Listings of comparative absorption spectra and transient absorption spectra. This material is available free of charge via the Internet at http://pubs.acs.org.

AUTHOR INFORMATION

Corresponding Author

*E-mail: meyer@jhu.edu.

Notes

The authors declare no competing financial interest.

ACKNOWLEDGMENTS

The National Science Foundation (CHE-1213357) is gratefully acknowledged for research support.

REFERENCES

(1) Vallee, B. L.; Williams, R. J. P. *Proc. Natl. Acad. Sci. U.S.A.* **1968**, *59*, 498−505.

(2) Lancaster, K. M.; Sproules, S.; Palmer, J. H.; Richards, J. H.; Gray, H. B. *J. Am. Chem. Soc.* **2010**, *132*, 14590−14595.

(3) Concepcion, J. J.; House, R. L.; Papanikolas, J. M.; Meyer, T. J. *Proc. Natl. Acad. Sci. U.S.A.* **2012**, *109*, 15560−15564.

(4) Kim, D.; Kirmaier, C.; Holten, D. *Chem. Phys.* **1983**, *75*, 305−322.

(5) Momenteau, M.; Reed, C. A. *Chem. Rev.* **1994**, *94*, 659−698.

(6) Traylor, T. G. *Acc. Chem. Res.* **1981**, *14*, 102−109.

(7) Wilson, E. K.; Bellelli, A.; Liberti, S.; Arese, M.; Grasso, S.; Cutruzzola, F.; Brunori, M.; Brzezinski, P. *Biochemistry* **1999**, *38*, 7556−7564.

(8) Monat, J. E.; McCusker, J. K. *J. Am. Chem. Soc.* **2000**, *122*, 4092−4097.

(9) Benko, G.; Kallioinen, J.; Korppi-Tommola, J. E. I.; Yartsev, A. P.; Sundstrom, V. *J. Am. Chem. Soc.* **2002**, *124*, 489−493.

(10) Hannappel, T.; Burfeindt, B.; Storck, W.; Willig, F. *J. Phys. Chem. B* **1997**, *101*, 6799−6802.

(11) Tachibana, Y.; Haque, S. A.; Mercer, I. P.; Durrant, J. R.; Klug, D. R. *J. Phys. Chem. B* **2000**, *104*, 1198−1205.

(12) Listorti, A.; O'Regan, B.; Durrant, J. R. *Chem. Mater.* **2011**, *23*, 3381−3399.

(13) Achey, D.; Ardo, S.; Xia, H.-L.; Siegler, M. A.; Meyer, G. J. *J. Phys. Chem. Lett.* **2011**, *2*, 305−308.

(14) Ferrere, S.; Gregg, B. A. *J. Am. Chem. Soc.* **1998**, *120*, 843−844.

(15) Morris, A. J.; Stromberg, J. R.; Meyer, G. J. *Inorg. Chem.* **2010**, *49*, 29−37.

(16) Duval, H.; Bulach, V.; Fischer, J.; Weiss, R. *Inorg. Chem.* **1999**, *38*, 5495−5501.

(17) Cedervall, P. E.; Dey, M.; Li, X.; Sarangi, R.; Hedman, B.; Ragsdale, S. W.; Wilmot, C. M. *J. Am. Chem. Soc.* **2011**, *133*, 5626−5628.

(18) Ebner, S.; Jaun, B.; Goenrich, M.; Thauer, R. K.; Harmer, J. *J. Am. Chem. Soc.* **2010**, *132*, 567−575.

(19) Adler, A. D.; Longo, F. R.; Kampas, F.; Kim, J. *J. Inorg. Nucl. Chem.* **1970**, *32*, 2443−2445.

(20) Chang, D.; Malinski, T.; Ulman, A.; Kadish, K. *Inorg. Chem.* **1984**, *23*, 817−824.

(21) Heimer, T. A.; D'Arcangelis, S. T.; Farzad, F.; Stipkala, J. M.; Meyer, G. J. *Inorg. Chem.* **1996**, *35*, 5319−5324.

(22) Argazzi, R.; Bignozzi, C. A.; Heimer, T. A.; Castellano, F. N.; Meyer, G. J. *Inorg. Chem.* **1994**, *33*, 5741−5749.

(23) Bard, A. J.; Faulkner, L. R. *Electrochemical Methods—Fundamentals and Applications*; John Wiley & Sons, Inc.: New York, 2001

(24) Bisquert, J.; Fabregat-Santiago, F.; Mora-Sero, I.; Garcia-Belmonte, G.; Barea, E. M.; Palomares, E. *Inorg. Chim. Acta* **2008**, *361*, 684−698.

(25) Achey, D.; Ardo, S.; Meyer, G. J. *Inorg. Chem.* **2012**, *51*, 9865−9872.

(26) Hadadzadeh, H.; Mansouri, G.; Rezvani, A.; Khavasi, H. R.; Skelton, B. W.; Makha, M.; Charati, F. R. *Polyhedron* **2011**, *30*, 2535−2543.

(27) Schwarz, H. A.; Creutz, C.; Sutin, N. *Inorg. Chem.* **1985**, *24*, 433−439.

(28) Walker, F. A.; Hui, E.; Walker, J. M. *J. Am. Chem. Soc.* **1975**, *97*, 2390−2397.

(29) Ardo, S.; Achey, D.; Morris, A. J.; Abrahamsson, M.; Meyer, G. J. *J. Am. Chem. Soc.* **2011**, *133*, 16572−16580.

(30) Cotton, F. A.; Wilkinson, G. *Advanced Inorganic Chemistry*, 5th ed.; Wiley Interscience: New York, 1988.

(31) Venkataramani, S.; Jana, U.; Dommaschk, M.; Sonnichsen, F. D.; Tuczek, F.; Herges, R. *Science* **2011**, *331*, 445−448.

(32) Song, Y.; Haddad, R. E.; Jia, S.-L.; Hok, S.; Olmstead, M. M.; Nurco, D. J.; Schore, N. E.; Zhang, J.; Ma, J.-G.; Smith, K. M.; Gazeau, S.; Pecaut, J.; Marchon, J.-C.; Medforth, C. J.; Shelnutt. *J. Am. Chem. Soc.* **2005**, *127*, 1179−1192.

(33) Coyle, C. L.; Rafson, P. A.; Abbott, E. H. *Inorg. Chem.* **1973**, *12*, 2007−2010.

(34) Brault, D.; Rougee, M. *Biochemistry* **1974**, *13*, 4591−4597.

(35) Drain, C. M.; Gentemann, S.; Roberts, J. A.; Nelson, N. Y.; Medforth, C. J.; Jia, S.; Simpson, M. C.; Smith, K. M.; Fajer, J.; Shelnutt, J. A.; Holten, D. *J. Am. Chem. Soc.* **1998**, *120*, 3781−3791.

(36) Retsek, J. L.; Drain, C. M.; Kirmaier, C.; Nurco, D. J.; Medforth, C. J.; Smith, K. M.; Sazanovich, I. V.; Chirvony, V. S.; Fajer, J.; Holten, D. *J. Am. Chem. Soc.* **2003**, *125*, 9787−9800.

(37) Thies, S.; Bornholdt, C.; Kohler, F.; Sonnichsen, F. D.; Nather, C.; Tuczek, F.; Herges, R. *Chem.—Eur. J.* **2010**, *16*, 10074−10083.

(38) Chen, L. X.; Zhang, X.; Wasinger, E. C.; Lockard, J. V.; Stickrath, A. B.; Mara, M. W.; Attenkofer, K.; Jennings, G.; Smolentsev, G.; Soldatov, A. *Chem. Sci.* **2010**, *1*, 642−650.

(39) O'Regan, B.; Gratzel, M. *Nature* **1991**, *353*, 737−740.

(40) Morris, A. J.; Marton, A.; Meyer, G. J. *Inorg. Chem.* **2008**, *47*, 7681−7685.

(41) Xia, H.-L.; Ardo, S.; Narducci-Sarjeant, A. A.; Huang, S.; Meyer, G. J. *Langmuir* **2009**, *25*, 13641−13652.

(42) Suzuki, H.; Adachi, H.; Miyazaki, Y.; Hoshino, M. *J. Phys. Chem. A* **2003**, *107*, 4445−4451.

(43) Hoshino, M. *Inorg. Chem.* **1986**, *25*, 2476−2478.

(44) Makarska-Bialokoz, M.; Pratviel, G.; Radzki, S. *J. Mol. Struct.* **2008**, *875*, 468−477.

(45) Hu, K.; Robson, K. C. D.; Johansson, P. J.; Berlinguette, C. P.; Meyer, G. J. *J. Am. Chem. Soc.* **2012**, *134*, 8352−8355.

(46) Robson, K. C. D.; Hu, K.; Meyer, G. J.; Berlinguette, C. P. *J. Am. Chem. Soc.* **2013**, *135*, 1961−1971.

(47) Nazeerudin, M. K.; Pechy, P.; Renouard, T.; Zakeeruddin, S. M.; Humphry-Baker, R.; Comte, P.; Liska, P.; Cevey, L.; Costa, E.; Shklover, V.; Spiccia, L.; Deacon, G. B.; Bignozzi, C. A.; Gratzel, M. *J. Am. Chem. Soc.* **2001**, *123*, 1613−1624.

(48) Zamyatin, A. V.; Gusev, A. V.; Rodgers, M. A. J. *J. Am. Chem. Soc.* **2004**, *126*, 15934−15935.

(49) Qu, P.; Thompson, D. W.; Meyer, G. J. *Langmuir* **2000**, *16*, 4662−4671.

(50) Liu, F.; Meyer, G. J. *Inorg. Chem.* **2003**, *42*, 7351−7353.

(51) Allsop, S. R.; Cox, A.; Kemp, T. J.; Reed, W. J. *J. Chem. Soc., Faraday Trans.* **1978**, *74*, 1275.

(52) Lumpkin, R. S.; Kober, E. M.; Worl, L. A.; Murtaza, Z.; Meyer, T. J. *J. Phys. Chem.* **1990**, *94*, 239−243.

(53) Maruszewski, K.; Strommen, D. P.; Kincaid, J. R. *J. Am. Chem. Soc.* **1993**, *115*, 8345−8350.